

We are IntechOpen, the world's leading publisher of Open Access books Built by scientists, for scientists

6,100

Open access books available

149,000

International authors and editors

185M

Downloads

Our authors are among the

154

Countries delivered to

TOP 1%

most cited scientists

12.2%

Contributors from top 500 universities



WEB OF SCIENCE™

Selection of our books indexed in the Book Citation Index
in Web of Science™ Core Collection (BKCI)

Interested in publishing with us?
Contact book.department@intechopen.com

Numbers displayed above are based on latest data collected.
For more information visit www.intechopen.com



A Dexterous Workspace Optimization for Ten Different Types of General Stewart-Gough Platforms

Burak Inner and Serdar Kucuk

Abstract

In this chapter, a dexterous workspace optimization is performed for ten different types of 6-Degrees-Of-Freedom (DOF) General Stewart-Gough Platforms (GSPs). The optimization aims to find the optimum radius of the circumferential circle and separation angles between adjacent vertices of base and moving platforms in order to maximize both the dexterities and workspaces of the manipulators subject to geometric constraints. Particle Swarm Optimization (PSO), increasingly being applied to engineering applications, is used as the optimization algorithm. Finally, the optimization results for ten different types of 6-DOF GSPs are compared to each other in terms of kinematic performances.

Keywords: general Stewart-Gough platforms, dexterous workspace optimization, particle swarm optimization, kinematic performance, stroke length, workspace

1. Introduction

Parallel robot manipulators are closed-loop mechanisms where all links are connected to the base and moving platform at the same time. They have potential advantages over serial robot manipulators such as high rigidity, compact size, high load capacity, fast response, and high precision [1–4]. Basically, parallel manipulators can be classified into two main categories, namely planar and spatial parallel manipulators. The first category composes of planar parallel manipulators which have simple structures and translate along x- and y-axes, and rotate around the z-axis, only. The second category includes spatial parallel manipulators that have 3 to 6-DOF, and can translate and rotate in the three-dimensional space. Stewart-Gough Platforms included in the second group are receiving increased interest from the robotics community and industry recently. They have been used in many potential applications such as multi-axis machine tools earthquake simulators, solar panels, radar antennas, telescopes, walking machines, micromanipulators, and surgery operations [5–7].

Several authors provided valuable contributions to the dimensional optimization of Stewart-Gough Platforms. Some important publications can be given as follows. Pittens and Podhorodeski [8] studied optimizing the local dexterity of a small group of

Stewart platform manipulators. Stoughton and Arai [9] designed a novel structure for the Stewart Platform manipulator. They also optimized the new structure considering both dexterity and workspace volume, and compared the novel structure with the traditional Stewart-Gough Platform in terms of dexterity. Du Plessis and Snyman [10] presented an optimization method for determining the dexterous workspaces of parallel manipulators. They applied the new method for the computation of dexterous workspaces of both planar and spatial Stewart-Gough platforms. Su et. al. [11] conducted a study about optimizing the structural characteristics of the Stewart platform for a large spherical radio telescope using genetic algorithms. They used the condition number of the Jacobian matrix as the objective function and radius of the base platform, adjacent actuator attachment points, and the distance between base and moving platforms as optimization variables. Yao [12] et al. performed the dimensional optimization of the Stewart-Gough platform for a five-hundred-meter aperture spherical radio telescope. The operability and accuracy of the Stewart-Gough platform are the main design objectives of their optimization problem. Mishra and Omkar [13] used different types of evolutionary algorithms (such as particle swarm optimization, genetic algorithm, variants, and simulated annealing) to present a model for singularity analysis of a 6-DOF Stewart-Gough Platform manipulator for precision and surgery. Jiang [14] completed a Ph.D. dissertation about singularity analysis and geometric optimization of two different kinds of parallel mechanisms namely, planar 3-RPR and spatial Stewart-Gough parallel manipulators. An algorithm for optimizing the geometric parameters is developed in order to maximize the singularity-free orientation workspace of the Stewart-Gough platform taking leg length ranges into account. Jiang and Gosselin [15] analyzed the effects of the orientation angles on the singularity-free workspace of the 3x3 Gough-Stewart platform in order to determine the optimal orientation. The same authors also studied the effects of the geometric parameters on the singularity-free workspace in order to determine the optimal architecture for the minimal simplified symmetric manipulator 3x3 Gough-Stewart platform [16]. Furthermore, they analyzed the maximal singularity-free total orientation workspace of the 3x3 Gough-Stewart platform [17].

Although there have been several studies about the optimization of Stewart-Gough platform manipulators in the literature, most of these studies have been restricted to 6-legged 3x3, 6x3, and 6x6 Stewart platform manipulators only. The study in this chapter presents a dexterous workspace optimization of all possible types of 6-legged architectures having five different prismatic active actuator stroke lengths between the base and moving platforms. These architectures consist of commonly used ten different types of Stewart-Gough platforms, namely the 6-DOF 3x3, 4x3, 4x4, 5x3, 5x4, 5x5, 6x3, 6x4, 6x5, and 6x6 parallel mechanisms as shown in **Figure 1**. The dexterities and workspaces of the 6-DOF Stewart-Gough platforms are used as the objective function subject to geometric constraints. The radius of the circumferential circles and separation angle between adjacent vertices of the base and moving platforms are considered as the optimization variables. A Particle Swarm Optimization (PSO) algorithm which is increasingly being applied in various engineering applications (wireless sensor networks [18], electromagnetics [19], biomedical [20], electronics [21], control [22], and robotics [23]), is used as the optimization tool. In general, a PSO algorithm can be implemented easily and it is computationally inexpensive in terms of both memory requirements and CPU time. It has been proven to be effective for especially dynamic optimization problems with multi-dimensional search spaces [24–28]. Finally, the optimization results for ten different types of 6-DOF GSPs with five different actuator stroke lengths are compared to each other and ranked in terms of kinematic performances.

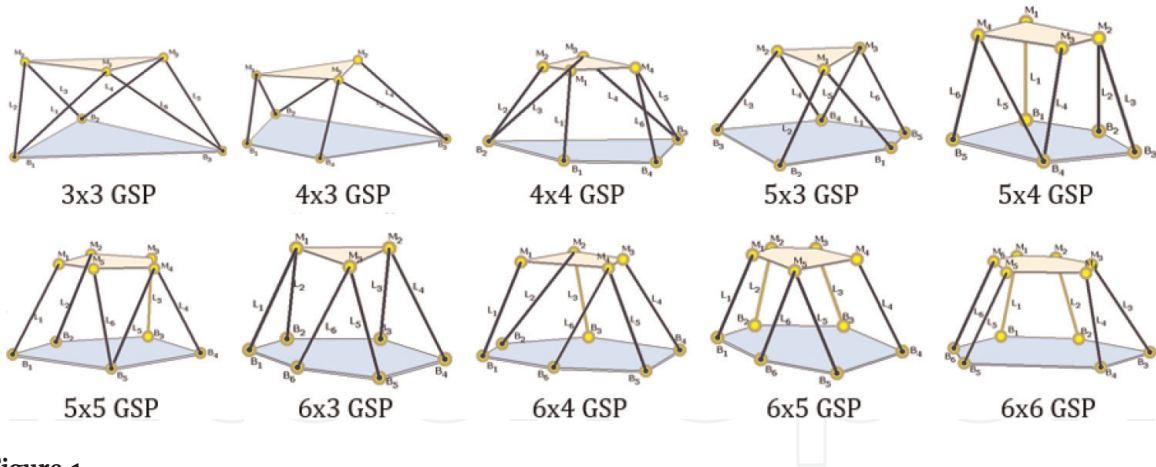


Figure 1. 6-DOF 3x3, 4x3, 4x4, 5x3, 5x4, 5x5, 6x3, 6x4, 6x5, 6x6 Stewart-Gough platforms.

2. Background

Geometric description, inverse kinematics, and Jacobian matrix derivations of 6-legged GSPs are explained in this section.

2.1 Geometric description of 6-legged GSPs

The possible structures for Stewart-Gough platform mechanisms with 6-legs are constructed by providing six active actuators between the base and moving platforms and 12 passive joints attached to both ends of each active actuator [14]. While the passive joints might be selected as spherical or universal joints, the active actuators are chosen as prismatic joints only. As stated in the introduction Section, the ten different types of 6-legged Stewart-Gough platform mechanisms can be constructed by changing the placements of the attachment points on the fixed base and moving platforms. For instance, in order to construct a 6-legged 3x3 Stewart platform shown in **Figure 2a**, the six legs are connected to both moving and base platforms at three attachment points while a 6-legged 6x6 Stewart-Gough platform illustrated in **Figure 2b** requires six attachment points at the base and moving platforms. In general to perform kinematic and dynamic operations, two reference coordinate frames namely $B=\{X, Y, Z\}$ and $M=\{x, y, z\}$ are attached to the centers of the base (O) and moving platforms (P), respectively. The passive joints are connected to B_i and M_i attachment points ($i=1, 2, 3$ for 3x3 of GSP and $i=1, 2 \dots 6$ 6x6 of GSP) on the fixed base and moving platform, respectively. The $B_i = [b_{ix} \ b_{iy} \ b_{iz}]^T$ and $M_i = [m_{ix} \ m_{iy} \ m_{iz}]^T$ are the position vectors of the points B_i and M_i in the B and M coordinate systems, respectively. The ψ_{b_i} and ψ_{m_i} illustrate the separation angles between adjacent vertices ($i=1, 2, 3$ for 3x3 of GSP and $i=1, 2 \dots 6$ 6x6 of GSP) of base and moving platforms, respectively.

2.2 Inverse kinematics and Jacobian matrix

The inverse kinematics of the GSPs can be determined by using the following equation when the position $P = [p_x \ p_y \ p_z]^T$ and orientation matrix $R_{XYZ}(\alpha, \beta, \gamma)$ of the end-effector in terms of base coordinate frames are given as

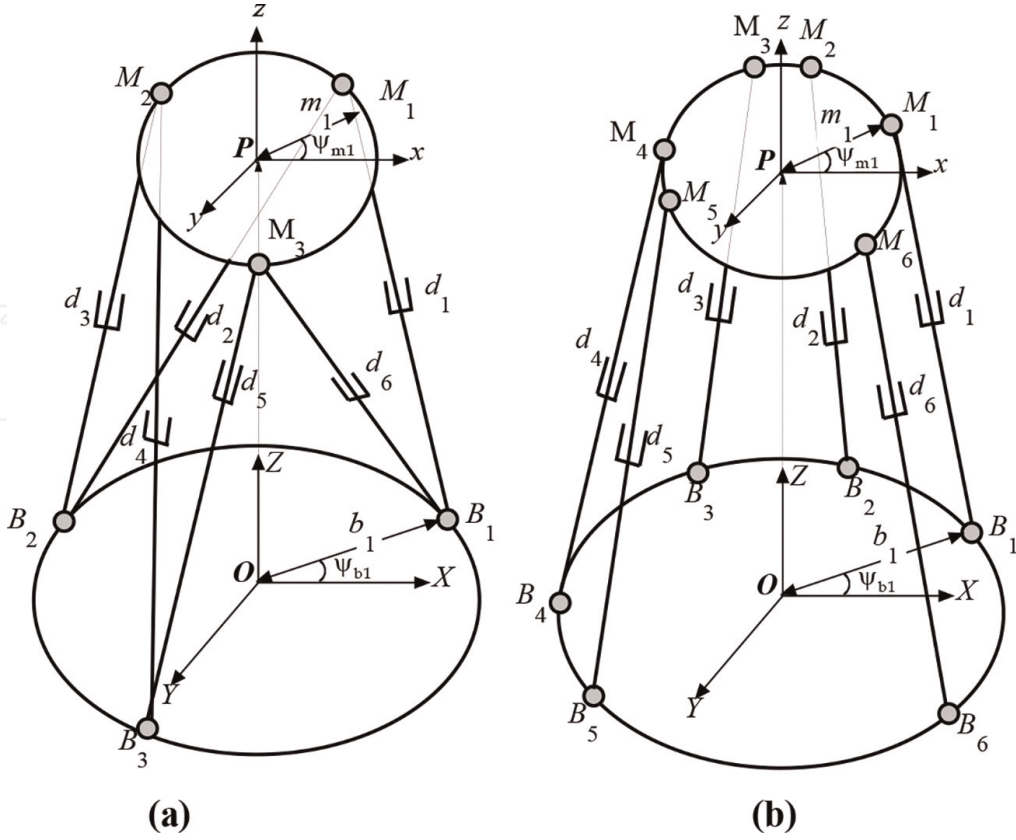


Figure 2.
 (a) The 6-legged 3x3 of GSP. (b) The 6-legged 6x6 of GSP.

$$d_i = R_{XYZ}M_i + P - B_i, i = 1,2,\dots,6 \quad (1)$$

where d_i denotes the active link lengths. The Jacobian matrix can be derived by applying the loop-closure equation to each limb.

$$\overrightarrow{OP} + \overrightarrow{PM}_i = \overrightarrow{OB} + \overrightarrow{B_iM_i}, i = 1,2,\dots,6 \quad (2)$$

where i equals the number of limbs. Differentiating Eq. (2) with respect to the time and eliminating the angular velocity of the active actuators with respect to the base frame in the resultant equation, the following identity is found [1].

$$z_i \cdot v_p + (m_i \times z_i) \cdot \omega_p = \dot{d}_i, i = 1,2,\dots,6 \quad (3)$$

where v_p , ω_p and \dot{d}_i are the linear and angular velocities of the moving platform and the linear velocities of active actuators, respectively. The term z_i denotes the unit vector along B_iM_i . Eq. (3) can be stated as

$$J_A \cdot \dot{\mathbf{x}} = J_B \cdot \dot{\mathbf{q}}, i = 1,2,\dots,6 \quad (4)$$

where $\dot{\mathbf{x}} = [v_p \ \omega_p]^T = [v_{p_x} \ v_{p_y} \ v_{p_z} \ \dot{\alpha} \ \dot{\beta} \ \dot{\gamma}]^T$, $\dot{\mathbf{q}} = [\dot{d}_1, \dot{d}_2, \dots, \dot{d}_6]^T$, J_B is equal to the 6x6 identity matrix and J_A is as follows.

$$J_A = \begin{bmatrix} z_1^T & m_1 \times z_1 \\ z_2^T & m_2 \times z_2 \\ z_3^T & m_3 \times z_3 \\ z_4^T & m_4 \times z_4 \\ z_5^T & m_5 \times z_5 \\ z_6^T & m_6 \times z_6 \end{bmatrix} \quad (5)$$

The overall Jacobian matrix is obtained as

$$J = J_B^{-1} J_A \quad (6)$$

3. Optimization constraints

The optimization problem is evaluated by taking some important geometric constraints into account. The geometric constraints include the minimum and maximum radii of the circumferential circles and separation angles between adjacent vertices which determine the connection points of the legs both on the base and the moving platforms, respectively.

The first geometric constraint is the minimum and maximum radii of the circumferential circles of the base and moving platforms. The minimum limits of the circumferential circles can be obtained by considering the physical dimensions of the passive joints (such as universal and spherical joints). **Figure 3** illustrates the placements of the passive joints on the base and moving platform for providing the physically minimum radii of the circumferential circles. The radius of the joints and the distance between two consecutive passive joints are denoted as r_j and j_m , respectively. The minimum limits of the circumferential circles ($r_{b(min)}$) depicted in **Figure 3** are determined by considering the radius of passive universal joints (r_j) and the distance between two consecutive passive joints (j_m). **Table 1** gives the minimum limits of the circumferential circles of the base and moving platform for 3 to 6-legged GSP mechanisms. The maximum radius of the circumferential circles of the base ($r_{b,max}$) and moving ($r_{m,max}$) platforms can be chosen based on the design requirements.

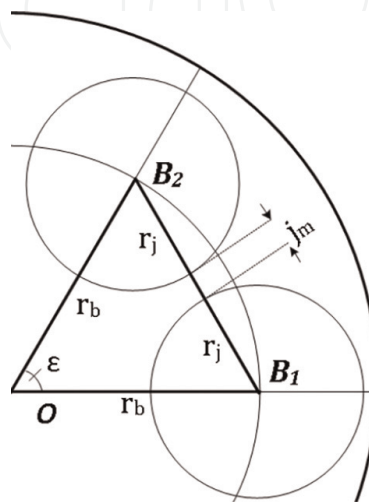


Figure 3.
 The minimum radius of the circumferential circles.

Number of connection points	3	4	5	6
Maximum angle (ϵ)	120°	90°	72°	60°
Minimum radius of the platform	$\frac{2r_j + j_m}{2 \sin(60)}$	$\frac{2r_j + j_m}{2 \sin(45)}$	$\frac{2r_j + j_m}{2 \sin(36)}$	$\frac{2r_j + j_m}{2 \sin(30)}$

Table 1.

Maximum separation angle for a minimum radius of the base and moving platforms.

The second geometric constraint is the separation angles between adjacent vertices which determine the connection points of the legs both on the base and moving platforms, respectively. The connection points refer to the centers of the passive joints whose coordinates are denoted as B_i on the base and M_i on the moving platforms, respectively. The minimum separation angle depends on the radius of the circumferential circles of the base or moving platforms. Since the radius of the passive joints is constant, as the radius of the circumferential circle gets larger, the separation angle becomes smaller as shown in **Figure 4**. The minimum separation angle for the base and moving platform is computed by using the cosines theorem on OB_1B_2 and PM_1M_2 triangle where the radius of the base and moving platforms denotes as r_b and r_m , respectively. $\delta_{b,min}$ and $\delta_{m,min}$ can be extracted as

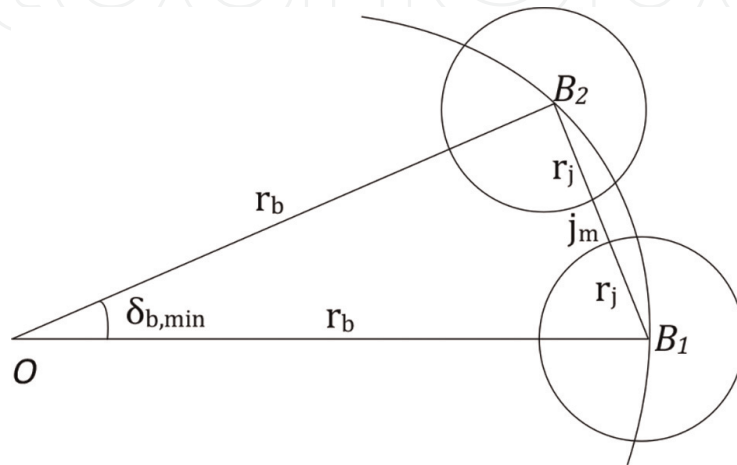
$$\delta_{bi,min} = \cos^{-1} \left(1 - \frac{(2r_j + j_m)^2}{2r_b^2} \right) \quad i = 1, 2, \dots, 6 \quad (7)$$

$$\delta_{mi,min} = \cos^{-1} \left(1 - \frac{(2r_j + j_m)^2}{2r_m^2} \right) \quad i = 1, 2, \dots, 6 \quad (8)$$

The following statement can be easily written since Eqs. (7) and (8) are the common identities for the minimum separation angles on the base and moving platforms, respectively.

$$\delta_{bi+1,min} = \delta_{bi,min} \quad i = 1, 2, \dots, 5. \quad (9)$$

$$\delta_{mi+1,min} = \delta_{mi,min} \quad i = 1, 2, \dots, 6 \quad (10)$$

**Figure 4.**

The illustration of the minimum separation angles.

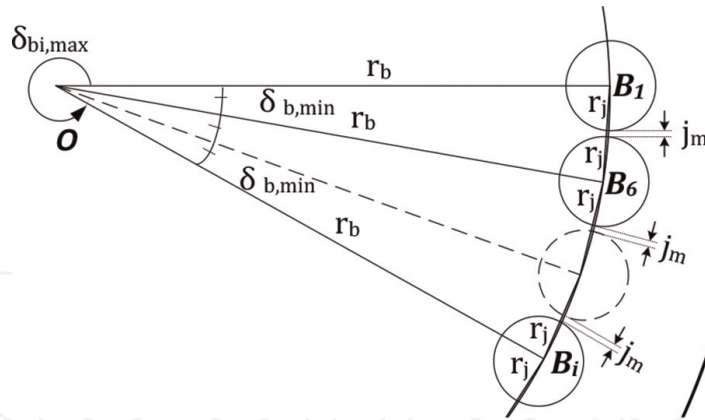


Figure 5.
 The illustration of the maximum separation angles.

Number of legs	3	4	5	6
Maximum angle (ϵ)	$360 - (4-i)\delta_{b,min}$	$360 - (5-i)\delta_{b,min}$	$360 - (6-i)\delta_{b,min}$	$360 - (7-i)\delta_{b,min}$

Table 2.
 The maximum separation angles of the base and moving platforms for GSPs.

The maximum separation angles of the base ($\delta_{bi,max}$) and moving ($\delta_{mi,max}$) platforms can be found considering the **Figure 5**. **Table 2** illustrates the maximum separation angles of the base ($\delta_{bi,max}$) and moving ($\delta_{mi,max}$) platforms for 3 to 6 legged GSPs. The separation angles (δ_{bj}, δ_{mj}) of the base and moving platforms are randomly chosen between the minimum angle denoted by Eqs. (7) and (8), and the maximum angle stated by **Table 2**, respectively where j is the number of legs that vary between 3 and 6.

4. Optimization objectives

In this optimization problem, the dexterities and workspaces of the manipulators are used as the optimization objectives subject to geometric constraints. Dexterity is a very important measure that directly affects the kinematic performance of robotic manipulators. The capability of achieving small displacements in arbitrary directions in the manipulator workspace [29] can be described as dexterity. There are some local and global dexterity measures based on the Jacobian matrix [30–32]. It should be noted that dexterity based on the Jacobian matrix may not directly be computed due to the dimensional inconsistencies of the matrix elements. Therefore a characteristic length is determined to homogenize the elements of the Jacobian matrix since the first three columns of the matrix J_A given by Eq. (5) have the units of length, whereas the last three columns have the units of length².

$$J_{AH} = \begin{bmatrix} J_{A1} & \frac{1}{L}J_{A2} \end{bmatrix} \quad (11)$$

where J_{AH} is the homogenized Jacobian matrix of J_A . The J_{A1} and J_{A2} are the 6×3 submatrices. The characteristic length L is determined as the radius of the moving platform. Thus the homogenized overall Jacobian matrix J_H is described as

$$J_H = J_B^{-1} J_{AH} \quad (12)$$

The local dexterity based on the condition number (κ) of the Jacobian matrix is given by

$$\kappa = \|J_H\| \|J_H^{-1}\| \quad (13)$$

where $\|\cdot\|$ illustrates the matrix norm as

$$\|J_H\| = \sqrt{\text{tr}(J_H n J_H^T)} \quad (14)$$

where n is a diagonal matrix. Condition number κ changes between 1 and ∞ . Inverse condition number $\eta = 1/\kappa$ limited between 0 and 1 is used in general to measure dexterity easily. The inverse condition number illustrates the local behavior of the manipulator. In order to measure the global property of the manipulator, Global Dexterity Index (GDI) is used as

$$GDI = \frac{\int_W \eta dW}{\int_W dW} \quad (15)$$

where the denominator of Eq. (15) illustrates the workspace volume of the manipulator. As the GDI approaches unity the manipulator gains better gross motion capability. The following identity can be used for GDI due to avoiding the troubles while computing the integrals in Eq. (15).

$$GDI = \frac{\sum \eta}{nmp} \quad (16)$$

where the nmp illustrates the number of points in the workspace and the numerator shows the sum of η values in the workspace grids.

Finally, the optimization problem for the ten different types of GSPs with five different actuator stroke lengths can be stated as the maximization of both the dexterities and workspaces of the manipulators subject to geometric constraints.

$$\text{Max GDI and Workspace} \quad (17)$$

Subject to

$$r_{b,min} \leq r_b \leq r_{b,max}$$

$$r_{m,min} \leq r_m \leq r_{m,max}$$

$$\delta_{bi,min} \leq \delta_{bi} \leq \delta_{bi,max} \quad i = 1, 2, \dots, 6.$$

$$\delta_{mi,min} \leq \delta_{mi} \leq \delta_{mi,max} \quad i = 1, 2, \dots, 6.$$

5. The particle swarm optimization

PSO is a robust stochastic optimization algorithm inspired by the biological social behavior of a swarm of birds or a school of fish. PSO was firstly introduced by

Kennedy and Eberhart in 1995 [33] while they have been attempting to simulate the motion of bird swarms. PSO is capable of finding optimal or near-optimal solutions in shorter computation time and also suitable for searching in large search space. Potential solutions within the search space are called particles and a population-based search is performed by considering the fitness values that are obtained from the positions of the particles. At each flight cycle, particles fly around in a multidimensional search space with a velocity, and the objective function is evaluated for each particle based on its position. Velocity directing the flight of particles is updated based on the particle's current velocity, the particle's own best fitness value and the global best fitness value of any particle in the population. Thus the movement of each particle is guided toward the local and the best-known positions in the search space. This is expected to move the swarm toward the best solutions.

PSO is started with a random population referred to as a swarm and search optima by updating generations iteratively. Each particle in the swarm is treated as a point in an N-dimensional search space and keeps track of the best solution (fitness) which has been achieved by that particle so far. The best solution is called as personal best (Pbest). The best value achieved up to now by any particle in the population is called as global best (Gbest). The basic concept of PSO lies in accelerating each particle toward its Pbest and the Gbest locations. The velocity of each particle in the swarm is updated by using the following equation. The performance and accuracy of the PSO algorithm are mostly based on the appropriate selection of constriction factor (χ), inertia weight (ω_k), and learning factors (c_1, c_2) parameters where k denotes the iteration number.

6. Simulation results

In this study, the kinematic structures of the ten GSPs are optimized for five different linear actuator stroke lengths. **Figure 6** illustrates a linear actuator whose extended length composes of stroke and retracted lengths. **Table 3** illustrates the joint radius (r_j), the stroke, retracted, and extended lengths of the linear actuators commonly used in industrial applications. According to **Table 3** the actuator stroke lengths change between 50mm and 250mm. In this study, the actuator stroke lengths are selected as 50mm, 100mm, 150mm, 200mm, and 250 mm, which are the common lengths used in industry. The radii of the passive joints that change between 13.5mm and 30mm with respect to the **Table 3** are selected as 18mm for five different stroke lengths. Finally, the distance between two consecutive passive joints is selected as 6mm in accordance with the commercial PI M⁻⁸⁴⁰.PD3 6-axis hexapod.

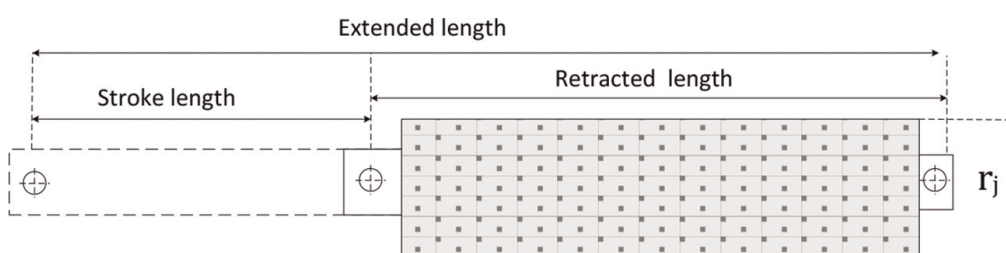


Figure 6.
Schematic diagram of a linear actuator.

Linear actuator	Model	Stroke length (mm)	Retracted length (mm)	Extended length (mm)	r_i (mm)
Oriental motor	DRL60PA4-05G	50	133	183	30
	DRL60PB4-10G	100	186.5	286.5	30
PI	M ⁻²³⁵ .5DG	50	218	268	13.5
Linear-Mech	LMI 02-C100	100	345	445	22.5
	LMI 02-C150	150	395	545	22.5
	LMI 02-C200	200	445	645	22.5
	LMI 02-C250	250	495	745	22.5
	LMP 03-C100	100	252	352	25
	LMP 03-C150	150	302	452	25
	LMP 03-C200	200	352	552	25
	LMP 03-C250	250	402	652	25

Table 3.
The stroke and retracted lengths of the linear actuators commonly used in industrial applications.

The three-dimensional Cartesian workspace volumes are planned such that the end-effectors of the ten GSPs with five different linear actuator stroke lengths can easily reach their own workspaces with the reference orientation angle $R_{XYZ}(\alpha, \beta, \gamma)$. **Table 4** illustrates the travel ranges of the orientation angles for the GSPs that have been generally used for industrial applications. The orientation angles of the moving platform are selected as $\alpha = \beta = \gamma = 0$ since the travel ranges of the commercial GSPs summarized in **Table 4** vary between very small intervals.

The minimum and maximum separation angles on the base and moving platform are the variables that can be calculated by using Eqs. (7), (8), and **Table 2**. In addition, **Table 5** illustrates the values of the minimum and maximum radii for base and moving platforms. The value of minimum radii for the base and moving platforms are computed as 42 by using **Table 1** while the maximum radii of the base and moving platforms given in **Table 5** are used with respect to the stroke lengths of the GSPs.

In this optimization problem, the individuals of a swarm are evaluated by considering the maximization of the objective functions stated by Eq. (17). For each generation, dexterities and workspaces of the ten different GSPs with five different linear

Manipulator	Travel range			Manipulator	Travel range		
	θ_x	θ_y	θ_z		θ_x	θ_y	θ_z
Newport HXP50	$\pm 9^\circ$	$\pm 8.5^\circ$	$\pm 18^\circ$	PI M-850KHLH	$\pm 3^\circ$	$\pm 3^\circ$	$\pm 4^\circ$
PI H-824	± 7.5	± 7.5	± 12.5	PI M-850KHLAH	$\pm 5^\circ$	$\pm 5^\circ$	$\pm 5^\circ$
PI M-811	$\pm 10^\circ$	$\pm 10^\circ$	$\pm 21^\circ$	SYMETRIE Bora	$\pm 15^\circ$	$\pm 15^\circ$	$\pm 15^\circ$
PI M-824.3DG	$\pm 7.5^\circ$	$\pm 7.5^\circ$	$\pm 12.5^\circ$	SYMETRIE Brevia	$\pm 15^\circ$	$\pm 15^\circ$	$\pm 15^\circ$
PI M-824.3PD	$\pm 7.5^\circ$	$\pm 7.5^\circ$	$\pm 12.5^\circ$	SYMETRIE Sonora	$\pm 2^\circ$	$\pm 2^\circ$	$\pm 2^\circ$

Table 4.
Orientation angles of GSPs used for industrial applications.

	Stroke 50 (in mm)		Stroke 100 (in mm)		Stroke 150 (in mm)		Stroke 200 (in mm)		Stroke 250 (in mm)	
	r_b	r_m	r_b	r_m	r_b	r_m	r_b	r_m	r_b	r_m
<i>min</i>	42	42	42	42	42	42	42	42	42	42
<i>max</i>	210	210	420	420	630	630	840	840	1050	1050

Table 5.
 The values of the minimum and maximum radii for base & moving platforms.

actuator stroke lengths are computed based on the radius of the circumferential circle, separation angles, and constant orientation angles of $\alpha = \beta = \gamma = 0$. The parameters of the PSO algorithm are selected as $\chi = 0.7298$, $c_1 = c_2 = 2.05$. The population size is selected as 40 particles. Each particle has composes of 13 elements. The objective function is evaluated for 60 generations.

The optimization results of ten different GSPs with five different linear actuator stroke lengths are shown in tables. Due to the page limitations, the optimization results of five GSPs are given only (**Tables 6–12**). The tables include the radius of the circumferential circles, separation angles between adjacent vertices, workspace volumes (WSP), GDI values, shapes of the base and moving platforms. The base and moving platforms are plotted in the same axes for easy comparison and illustrated as red and blue colors in the figures, respectively. The connection points of the legs on base and moving platforms, retracted and extracted lengths are also given in tables in order to show the data belonging to the manipulators in a compact form.

As can be seen in **Tables 6–12**, the radii of the base platforms are optimized larger than the radii of the moving platforms for each actuator stroke length of the ten different GSPs. The optimization results show that the locations of the connection points on the base platform form roughly a triangle. As the GSP mechanism with four connection points is taken into account, the location of the two connection points is optimized separately, while the locations of the last two consecutive connection points are optimized close to each other. These two close consecutive connection points can be considered as one connection point. Thus, a rough triangle forms with the first two connection points and the last two close consecutive connection points. There are one separate connection point and two close consecutive connection points for GSP mechanisms with five connection points that form a rough triangle base platform. Finally, the GSP mechanisms with six connection points form a rough triangle having three close consecutive connection points.

Most of the connection points on the moving platforms of the GSPs are located separately while the connection points on the moving platforms of the 4x4, 5x5, 6x5, and 6x6 GSP mechanisms are optimized as a roughly triangle like in the base platforms. The base and moving platforms of 6x5 and 6x6 GSPs are optimized as a rough equilateral triangle for each actuator stroke length. As can be seen in **Tables 6–12**, the GDI values of 6x5 and 6x6 GSPs are higher than the others. It can be concluded that the rough equilateral triangle structure for the base and moving platforms can produce better kinematic performance.

It can be concluded from **Tables 6–12** that as the actuator stroke lengths get longer the workspace of the GSPs become larger. However, the GDI values of the GSPs do not continuously increase as the actuator stroke lengths get longer. **Figure 7** illustrates the GDI values of the ten different GSPs for each actuator stroke length. As can be

Optimized design variables	Stroke lengths (in mm)						
	50	100	150	200	250		
Radius (in mm)	r_b	130.79	203.35	42.05	404.34	515.41	<p>Stroke length of 50</p>
	r_m	45.12	42.31	52.91	54.56	58.66	
Separation angles of the moving platform (in degrees)	δ_{m1}	0.00	0.00	172.60	92.54	93.93	<p>Stroke length of 100</p>
	δ_{m2}	121.13	118.83	293.20	211.15	212.92	
	δ_{m3}	239.13	238.69	105.57	314.73	318.05	
Separation angles of the base platform (in degrees)	δ_{b1}	36.16	38.85	105.57	0.00	0.00	<p>Stroke length of 150</p>
	δ_{b2}	159.30	158.09	224.28	113.46	113.97	
	δ_{b3}	275.31	279.59	345.77	230.19	231.21	
Retracted Length (in mm)	150	250	280	592	740	<p>Stroke length of 200</p>	
Extended Length (in mm)	200	350	430	792	990		
GDI	0.918	0.829	0.821	0.784	0.785		
WSP (in cm ³)	116.28	328.23	1133	1344.4	1550		
Connection points of the legs on base and moving platforms							<p>Stroke length of 250</p>
Legs	L_1	L_2	L_3	L_4	L_5	L_6	
Base	B_1	B_1	B_2	B_2	B_3	B_3	
Moving	M_3	M_1	M_1	M_2	M_3	M_1	

Table 6.
The optimization results for 3x3 GSP.

seen in **Figure 7** the actuator stroke length of 100mm has better GDI values for ten different GSPs in general. It can be noticed that the actuator stroke length of 150mm has very close GDI values to the actuator stroke length of 100mm. Moreover, the actuator stroke length of 150mm has a larger workspace than the actuator stroke

Optimized design variables	Stroke lengths (in mm)					
		50	100	150	200	250
Radius	r_h	154.75	200.28	231.15	411.20	520.90
	r_m	42.81	42.11	42.02	42.54	42.15
Separation angles of the moving platform (in degrees)	δ_{m1}	113.76	72.44	67.90	67.28	64.34
	δ_{m2}	207.78	185.25	185.13	187.36	184.83
	δ_{m3}	301.16	300.18	300.03	300.84	300.22
Separation angles of the base platform (in degrees)	δ_{b1}	0.00	0	0	0	0
	δ_{b2}	112.55	110.98	108.54	114.77	114.45
	δ_{b3}	208.72	235.65	233.95	236.84	236.28
	δ_{b4}	344.40	347.96	349.57	354.14	355.38
Retracted Length (in mm)		150	250	280	592	740
Extended Length (in mm)		200	350	430	792	990
GDI		0.745	0.829	0.821	0.784	0.785
WSP (in cm^3)		55.66	328.23	1133	1344.36	1550
Connection points of the legs on base and moving platforms						
Legs	L_1	L_2	L_3	L_4	L^5	L_6
Base	B_1	B_2	B_2	B_3	B_3	B_4
Moving	M_1	M_1	M_2	M_2	M_3	M_3

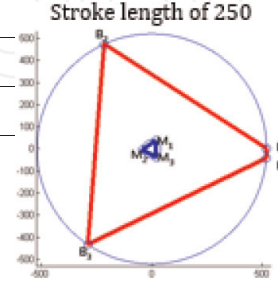
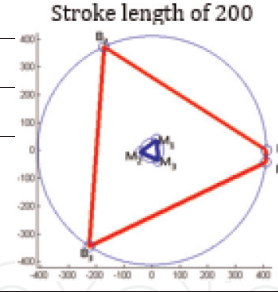
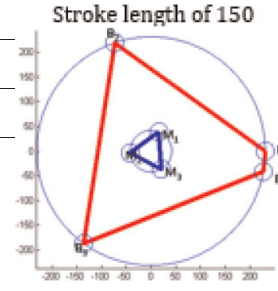
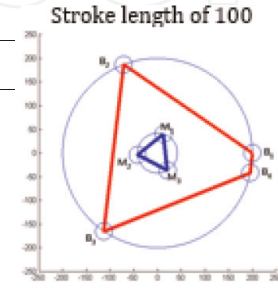
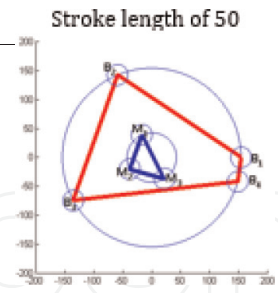


Table 7.
 The optimization results for 4×3 GSP.

length of 100mm. Thus, the designers can select the actuator stroke lengths of 100mm or 150mm considering the workspace requirements to construct GSPs with higher kinematic performances.

Optimized design variables		Stroke lengths						
		50	100	150	200	250		
Radius	r_b	157.13	204.43	234.16	406.02	528.65	<p>Stroke length of 50</p>	
	r_m	45.85	42.13	42.08	42.00	42.08		
Separation angles of the moving platform (in degrees)	δ_{m1}	123.13	70.68	70.18	64.01	64.48		<p>Stroke length of 100</p>
	δ_{m2}	216.98	190.25	189.85	185.09	186.00		
	δ_{m3}	305.48	300.19	300.12	299.97	300.12		
Separation angles of the base platform (in degrees)	δ_{b1}	0.91	0.00	0.00	0.00	0.00		<p>Stroke length of 150</p>
	δ_{b2}	114.22	104.85	107.22	114.38	117.46		
	δ_{b3}	129.58	116.64	117.51	120.31	122.01		
	δ_{b4}	217.21	234.90	230.17	237.56	240.87		
	δ_{b5}	343.54	348.20	349.71	354.07	355.36		
Retracted Length (in mm)		150	250	280	592	740	<p>Stroke length of 200</p>	
Extended Length (in mm)		200	350	430	792	990		
GDI		0.705	0.820	0.811	0.772	0.785		
WSP (cm ³)		58.20	290.20	1094.99	1399.52	1466.90		
Connection points of the legs on base and moving platforms							<p>Stroke length of 250</p>	
Legs	L ₁	L ₂	L ₃	L ₄	L ₅	L ₆		
Base	B ₁	B ₂	B ₃	B ₄	B ₄	B ₅		
Moving	M ₁	M ₁	M ₂	M ₂	M ₃	M ₃		

Table 8.
The optimization results for 5x3 GSP.

The kinematic performances of the ten different GSPs are compared by their actuator stroke length. The GDI values of GSPs for each actuator stroke length given by **Table 13** are sorted out from the highest to the lowest. Comparisons show that the best manipulators for each actuator stroke length are 6x5 and 6x6 GSP mechanisms

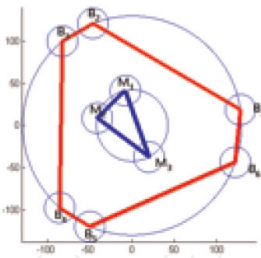
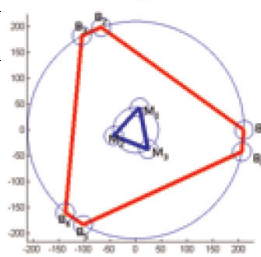
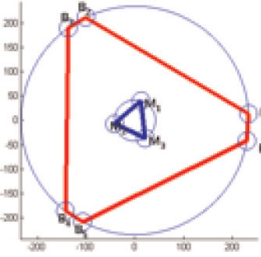
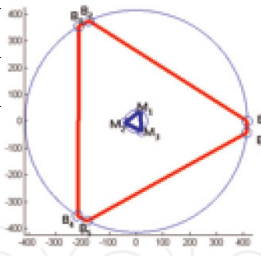
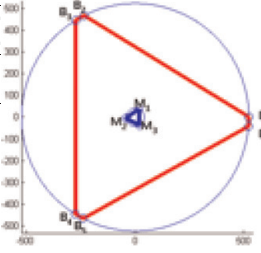
Optimized design variables		Stroke lengths					
		50	100	150	200	250	
Radius	r_b	129.45	210.49	234.74	414.76	524.13	 <p>Stroke length of 50</p>
	r_m	42.18	44.12	42.31	42.17	42.02	
Separation angles of the moving platform (in degrees)	δ_{m1}	100.90	80.31	72.75	68.69	64.91	 <p>Stroke length of 100</p>
	δ_{m2}	167.76	194.47	189.30	187.28	185.40	
	δ_{m3}	298.10	303.15	300.47	300.26	300.02	
Separation angles of the base platform (in degrees)	δ_{b1}	8.39	0.00	3.34	0.00	0.01	 <p>Stroke length of 150</p>
	δ_{b2}	110.98	108.50	115.52	115.16	116.84	
	δ_{b3}	129.65	119.95	125.79	120.97	121.43	
	δ_{b4}	228.59	229.40	232.40	238.17	238.17	
	δ_{b5}	247.26	240.85	242.66	243.98	242.81	
	δ_{b6}	340.51	348.53	349.67	354.04	355.40	
Retracted Length (in mm)		150	250	280	592	740	 <p>Stroke length of 200</p>
Extended Length (in mm)		200	350	430	792	990	
GDI		0.642	0.811	0.791	0.771	0.776	
WSP (cm ³)		56.88	250.09	1099.23	1309.14	1514.48	
Connection points of the legs on base and moving platforms							 <p>Stroke length of 250</p>
Legs	L_1	L_2	L_3	L_4	L_5	L_6	
Base	B_1	B_2	B_3	B_4	B_5	B_6	
Moving	M_1	M_1	M_2	M_2	M_3	M_3	

Table 9.
 The optimization results for 6x3 GSP.

whose lower and upper bounds of GDI values change between 0.883 and 0.928, respectively. The physical meaning of these values is that the 6x5 and 6x6 manipulator structures provide better dexterous maneuverability and kinematic performance than the others. These manipulators have also larger workspaces than those of the same

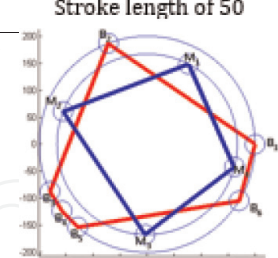
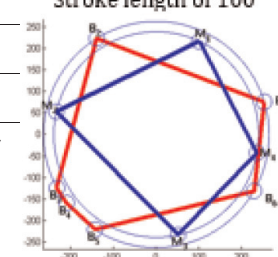
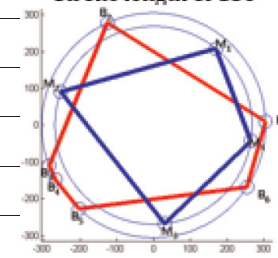
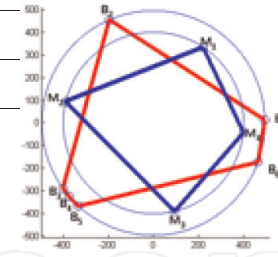
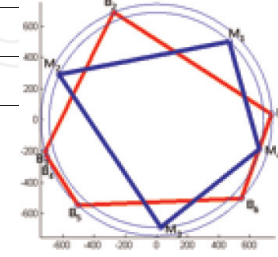
Optimized design variables	Stroke lengths						
	50	100	150	200	250		
Radius	r_b	168.19	263.47	304.97	494.46	741.16	 <p>Stroke length of 50</p>
	r_m	144.04	239.37	268.54	399.81	687.17	
Separation angles of the moving platform (in degrees)	δ_{m1}	63.16	65.25	50.65	56.58	47.02	 <p>Stroke length of 100</p>
	δ_{m2}	157.35	167.07	160.31	166.37	155.03	
	δ_{m3}	260.59	282.24	276.55	283.37	272.38	
	δ_{m4}	343.04	349.76	350.91	353.90	344.17	
Separation angles of the base platform (in degrees)	δ_{b1}	0.00	16.74	1.91	1.45	2.86	 <p>Stroke length of 150</p>
	δ_{b2}	109.09	121.81	114.27	113.35	111.73	
	δ_{b3}	198.28	208.17	201.04	215.69	195.59	
	δ_{b4}	212.63	217.31	208.93	220.56	198.88	
	δ_{b5}	227.02	237.11	228.21	227.64	227.19	
	δ_{b6}	322.44	330.06	326.60	339.69	317.50	
Retracted Length (in mm)	150	250	280	592	740	 <p>Stroke length of 200</p>	
Extended Length (in mm)	200	350	430	792	990		
GDI	0.864	0.822	0.822	0.781	0.786		
WSP (cm ³)	62.56	651	1415	1502	1586		
Connection points of the legs on base and moving platforms							 <p>Stroke length of 250</p>
Legs	L ₁	L ₂	L ₃	L ₄	L ₅	L ₆	
Base	B ₁	B ₂	B ₃	B ₄	B ₅	B ₆	
Moving	M ₁	M ₂	M ₂	M ₃	M ₄	M ₄	

Table 10.
The optimization results for 6x4 GSP.

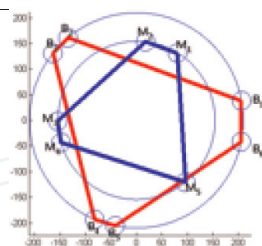
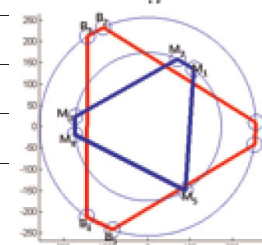
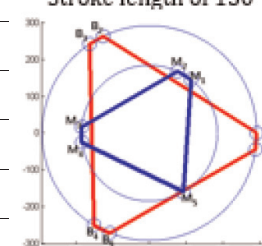
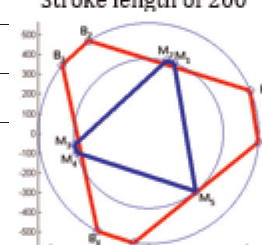
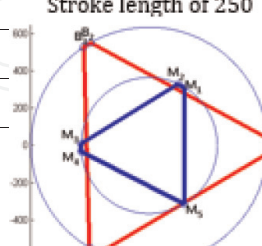
Optimized design variables		Stroke lengths					
		50	100	150	200	250	
Radius	r_b	209.95	256.18	334.88	561.02	635.39	 <p>Stroke length of 50</p>
	r_m	154.31	173.90	168.87	379.88	365.68	
Separation angles of the moving platforms (in degrees)	δ_{m1}	58.48	51.26	101.75	70.04	58.29	 <p>Stroke length of 100</p>
	δ_{m2}	83.37	65.95	117.10	76.40	64.93	
	δ_{m3}	180.54	172.20	131.39	188.63	178.31	
	δ_{m4}	196.26	186.10	231.68	195.02	184.91	
	δ_{m5}	308.59	300.46	345.71	308.83	300.66	
Separation angles of the moving platform (in degrees)	δ_{b1}	10.56	2.32	1.24	22.79	3.56	 <p>Stroke length of 150</p>
	δ_{b2}	129.96	114.27	119.10	123.07	119.67	
	δ_{b3}	141.44	123.93	232.00	141.77	123.65	
	δ_{b4}	247.00	235.64	239.19	242.34	239.74	
	δ_{b5}	258.49	250.94	256.19	262.16	245.06	
	δ_{b6}	346.24	350.59	351.80	355.45	356.21	
Retracted Length (in mm)		150	250	280	592	740	 <p>Stroke length of 200</p>
Extended Length (in mm)		200	350	430	792	990	
GDI		0.928	0.922	0.915	0.884	0.886	
WSP (cm ³)		106.9	741.2	1531.6	1620.0	1805.1	
Connection points of the legs on base and moving platforms							 <p>Stroke length of 250</p>
Legs	L_1	L_2	L_3	L_4	L_5	L_6	
Base	B_1	B_2	B_3	B_4	B_5	B_6	
Moving	M_1	M_2	M_3	M_4	M_5	M_6	

Table 11.
 The optimization results for 6x5 GSP.

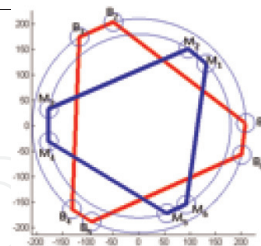
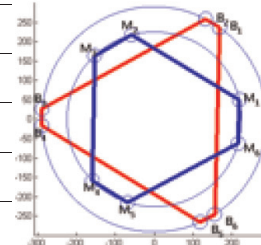
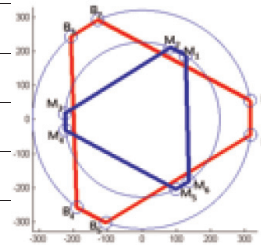
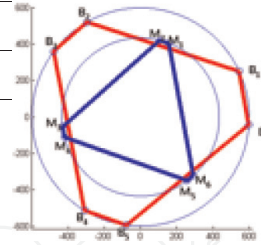
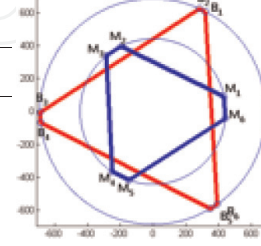
Optimized design variables		Stroke lengths					
		50	100	150	200	250	
Radius	r_b	205.81	290.40	320.49	599.12	688.71	Stroke length of 50 
	r_m	153.73	225.11	226.68	434.32	443.86	
Separation angles of the moving platform (in degrees)	δ_{m1}	0.00	13.00	56.05	68.94	11.88	Stroke length of 100 
	δ_{m2}	85.69	104.95	68.70	75.73	115.77	
	δ_{m3}	104.87	133.14	175.54	186.96	130.05	
	δ_{m4}	209.34	224.86	187.82	194.65	235.77	
	δ_{m5}	225.38	252.24	296.01	306.33	251.01	
	δ_{m6}	338.46	343.85	307.00	312.08	354.55	
Separation angles of the base platform (in degrees)	δ_{b1}	35.13	54.63	10.02	24.72	62.18	Stroke length of 150 
	δ_{b2}	46.84	62.92	113.89	119.63	65.82	
	δ_{b3}	156.76	174.66	130.56	143.06	180.36	
	δ_{b4}	168.89	183.27	233.35	239.03	185.53	
	δ_{b5}	269.71	294.13	250.63	262.41	300.64	
	δ_{b6}	284.75	302.43	351.92	355.88	304.74	
Retracted Length (in mm)		150	250	280	592	740	Stroke length of 200 
Extended Length (in mm)		200	350	430	792	990	
GDI		0.918	0.923	0.918	0.891	0.893	
WSP (cm3)		116.47	777	1558	1552	1738	
Connection points of the legs on base and moving platforms							Stroke length of 250 
Legs	L_1	L_2	L_3	L_4	L_5	L_6	
Base	B_1	B_2	B_3	B_4	B_5	B_6	
Moving	M_1	M_2	M_3	M_4	M_5	M_6	

Table 12.
The optimization results for 6x6 GSP.

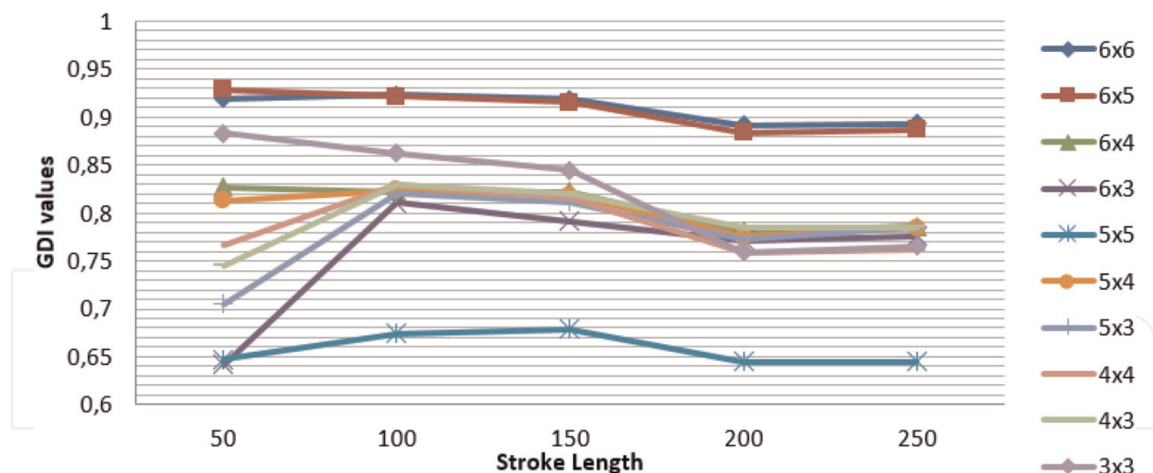


Figure 7.
 The GDI values of the ten different GSPs for each actuator stroke length.

actuator stroke lengths in **Tables 14**. The GDI values of 5x5 GSP mechanisms for each actuator stroke length vary between 0,645 and 0,678 which is the worst kinematic performance among the others. In addition, these manipulators have also smaller workspaces that might not be preferred by the designer for constructing their GSPs.

7. Conclusions

Ten different types of 6-DOF GSPs with five different actuator stroke lengths are optimized in this chapter. Dexterities and workspaces of the manipulators are considered as optimization objectives in order to obtain the radius of the circumferential circles, and separation angles between adjacent vertices of base and moving platforms. The PSO is used as the optimization algorithm. The optimization results of ten different GSPs with five different linear actuator stroke lengths are illustrated as tables that include the radius of the circumferential circle, separation angles between adjacent vertices, workspace volumes, GDI values, shapes of the base and moving platforms, retracted and extracted lengths of the linear actuators, and connection points of the legs on the base and moving platforms in order to show the data belonging to the manipulators in a compact form.

The optimizations produced the following important results. The radii of the base platforms are obtained larger than the radii of the moving platforms for GSPs with each actuator stroke length. The locations of the connection points on base platform form a rough triangle. The rough equilateral triangle structure for the base and moving platforms can produce the best kinematic performance like 6x5 and 6x6 GSP mechanisms. These manipulators have the best dexterous maneuverability and kinematic performance, and also the largest workspaces for each actuator stroke length. The actuator stroke lengths of 100mm and 150mm produce the best GDI values for ten different GSPs. The 5x5 GSP mechanisms for each actuator stroke length have the worst kinematic performance and smaller workspaces.

In practice, the designers and researchers can use the optimization results given in **Tables 6–14** to construct the optimal GSP mechanisms for the given specific tasks.

Stroke length 50				Stroke length 100				Stroke length 150			
Order	GSP	GDI	Workspace (in cm ³)	Order	GSP	GDI	Workspace (in cm ³)	Order	GSP	GDI	Workspace (in cm ³)
1	6x5	0.928	106.88	1	6x6	0.923	777.34	1	6x6	0.915	1558.02
2	6x6	0.919	116.47	2	6x5	0.921	741.16	2	6x5	0.914	1532.00
3	3x3	0.883	75.58	3	3x3	0.862	511.59	3	3x3	0.844	1346
4	6x4	0.827	87.23	4	4x4	0.830	131.88	4	6x4	0.821	1415
5	5x4	0.813	96.91	5	4x3	0.829	328.23	5	4x3	0.820	1133
6	4x4	0.767	48.26	6	5x4	0.823	669.90	6	5x4	0.818	1426
7	4x3	0.745	55.66	7	6x4	0.821	651.22	7	4x4	0.815	747
8	5x3	0.705	58.2	8	5x3	0.820	290.20	8	5x3	0.811	1095
9	5x5	0.648	30.69	9	6x3	0.810	250.09	9	6x3	0.791	1099
10	6x3	0.642	56.88	10	5x5	0.673	644.96	10	5x5	0.678	653

Table 13.
GSPs with stroke lengths of 50, 100, and 150.

Stroke length 50				Stroke length 100				Stroke length 150			
Order	GSP	GDI	Workspace (in cm ³)	Order	GSP	GDI	Workspace (in cm ³)	Order	GSP	GDI	Workspace (in cm ³)
1	6x5	0.928	106.88	1	6x6	0.923	777.34	1	6x6	0.915	1558.02
2	6x6	0.919	116.47	2	6x5	0.921	741.16	2	6x5	0.914	1532.00
3	3x3	0.883	75.58	3	3x3	0.862	511.59	3	3x3	0.844	1346
4	6x4	0.827	87.23	4	4x4	0.830	131.88	4	6x4	0.821	1415
5	5x4	0.813	96.91	5	4x3	0.829	328.23	5	4x3	0.820	1133
6	4x4	0.767	48.26	6	5x4	0.823	669.90	6	5x4	0.818	1426
7	4x3	0.745	55.66	7	6x4	0.821	651.22	7	4x4	0.815	747
8	5x3	0.705	58.2	8	5x3	0.820	290.20	3	5x3	0.811	1095
9	5x5	0.648	30.69	9	6x3	0.810	250.09	9	6x3	0.791	1099
10	6x3	0.642	56.88	10	5x5	0.673	644.96	10	5x5	0.678	653

Table 14.
GSPs with stroke length of 200, 250.

IntechOpen

Author details


Burak Inner¹ and Serdar Kucuk^{2*}

1 Engineering Faculty, Department of Computer Engineering, Kocaeli University, Kocaeli, Turkey

2 Technology Faculty, Department of Biomedical Engineering, Kocaeli University, Kocaeli, Turkey

*Address all correspondence to: skucuk@kocaeli.edu.tr

IntechOpen

© 2022 The Author(s). Licensee IntechOpen. This chapter is distributed under the terms of the Creative Commons Attribution License (<http://creativecommons.org/licenses/by/3.0>), which permits unrestricted use, distribution, and reproduction in any medium, provided the original work is properly cited. 

References

- [1] Tsai LW. Robot Analysis: The Mechanics of Serial and Parallel Manipulators. New York: John Wiley & Sons; 1999
- [2] Merlet JP. Parallel Robots. Netherlands: Kluwer Academic Publishers; 2000
- [3] Kang BH, Wen JT, Dagalakis NG, Gorman JJ. Analysis and design of parallel mechanisms with flexure joints. In: Proc. of IEEE International Conference on Robotics and Automation. New Orleans, LA, USA. 2004. pp. 4097-4102
- [4] Uchiyama M. Structures and characteristics of parallel manipulators. *Advanced Robotics*. 1994;**8**(6):545-557
- [5] Gao F, Li W, Zhao X, Jin Z, Zhao H. New kinematic structures for 2-, 3-, 4-, and 5-DOF parallel manipulator designs. *Mechanism and Machine Theory*. 2002;**37**(11):1395-1411
- [6] Gallardo-Alvarado J, Orozco-Mendoza H, Rico-Martínez JM. A novel five-degrees-of-freedom decoupled robot. *Robotica*. 2010;**28**(06):909-917
- [7] Li F, Kuiper JH, Khan SA, Hutchinson C, Evans CE. OC30 a new method to measure the inter-fracture site movement (IFMS) dynamically by means of Stewart platform manipulator algorithm. *Journal of Bone and Joint Surgery - British Volume*. 2008;**90-B** (SUPP II):366-367
- [8] Pittens and Podhorodeski. A family of Stewart platforms with optimal dexterity. *Journal of Robotic Systems*. 1993;**10**(4):463-479
- [9] Stoughton RS, Arai T. A modified Stewart platform manipulator with improved dexterity. *IEEE Transactions on Robotics and Automation*. 1993;**9**(2): 166-173
- [10] Du Plessis LJ, Snyman JA. A numerical method for the determination of dexterous workspaces of Gough–Stewart platforms. *International Journal for Numerical Methods in Engineering*. 2001;**52**:345-369
- [11] Su YX, Duan BY, Zheng CH. Genetic design of kinematically optimal fine tuning Stewart platform for large spherical radio telescope. *Mechatronics*. 2001;**11**:821-835
- [12] Yao R, Zhu WB, Yang QG. Dimension optimization design of the Stewart platform in FAST. *Advanced Materials Research*. 2011;**308–310**:2110-2113
- [13] Mishra A, Omkar SN. Singularity analysis and comparative study of six degree of freedom Stewart platform as a robotic arm by heuristic algorithms and simulated annealing. *International Journal of Engineering Science and Technology*. 2011;**3**(1)
- [14] Jiang Q. Singularity-Free Workspace Analysis and Geometric Optimization of Parallel Mechanisms. Québec: Université Laval; 2008
- [15] Jiang Q, Gosselin CM. Effects of orientation angles on the singularity-free workspace and orientation optimization of the Gough–Stewart platform. *Journal of Mechanisms and Robotics*. 2010;**2**: 011001-1
- [16] Jiang Q, Gosselin CM. Geometric optimization of the MSSM Gough–Stewart platform. *Journal of Mechanisms and Robotics*. 2009;**1**:031006-1
- [17] Jiang Q, Gosselin CM. Maximal singularity-free total orientation

workspace of the Gough–Stewart platform. *Journal of Mechanisms and Robotics*. 2009;**1**:034501-1

[18] Guru S, Halgamuge S, Fernando S. Particle swarm optimisers for cluster formation in wireless sensor networks. In: *Proceedings of the 2005 International Conference on Intelligent Sensors, Sensor Networks and Information Processing Conference*. Melbourne, VIC, Australia. 2005. pp. 319-324

[19] Rahmat-Sammi Y, Jin N, Xu S. Particle swarm optimization (pso) in electro-magnetics: Let the bees design your antennas. In: *22nd Annual Review on Progress in Applied Electromagnetics*. 2006

[20] Selvan S, Xavier C, Karssemeijer N, Sequeira J, Cherian R, Dhala B. Parameter estimation in stochastic mammogram model by heuristic optimization techniques. *IEEE Transactions on Information Technology in Biomedicine*. 2006;**10**(4):685-695

[21] Shi X, Yeo KS, Ma J-G, Do MA, Li E. Scalable model of on-wafer interconnects for high-speed CMOS ICs. *IEEE Transactions on Advanced Packaging*. 2006;**29**(4):770-776

[22] Kucuk S. Energy minimization for 3-RRR fully planar parallel manipulator using particle swarm optimization. *Mechanism and Machine Theory*. 2013;**62**:129-149

[23] Toz M, Kucuk S. Dexterous workspace optimization of an asymmetric six-degree of freedom Stewart–Gough platform type manipulator. *Robotics and Autonomous Systems*. 2013;**61**(12):1516-1528

[24] Kiranyaz S, Pulkkinen J, Gabbouj M. Multi-dimensional particle swarm optimization in dynamic environments. *Expert Systems with Applications*. 2011; **38**:2212-2223

[25] Angeline PJ. Tracking extrema in dynamic environments. In: *Proceedings of the 6th Conference on Evolutionary Programming*. Heidelberg: Springer-Verlag; 1997. pp. 335-345

[26] Kennedy J, Eberhart RC, Shi Y. *Swarm Intelligence*. New York: Morgan Kaufmann; 2001

[27] Aliyari MS, Teshnehlab M, Sedigh AK. A novel training algorithm in ANFIS structure. In: *Proceedings of American Control Conference*. Minneapolis, Minnesota; 2006

[28] Blackwell TM, Branke J. Multi-swarms, exclusion, and anticonvergence in dynamic environments. *IEEE Transactions on Evolutionary Computation*. 2004;**10**/4:51-58

[29] Kucuk S. A dexterity comparison for 3-DOF planar parallel manipulators with two kinematic chains using genetic algorithms. *Mechatronics*. 2009;**19**(6):868-877

[30] Klein CA, Blaho BE. Dexterity measures for the design and control of kinematically redundant manipulators. *The International Journal of Robotics Research*. 1987;**6**(2):72-83

[31] Gosselin C, Angeles J. A global performance index for the kinematic optimization of robotic manipulators. *Journal of Mechanisms and Robotics*. 1991;**113**:220-226

[32] Zanganeh EK, Angeles J. Kinematic isotropy and the optimum design of parallel manipulators. *The International Journal of Robotics Research*. 1997;**16**(2): 185-197

[33] Kennedy J, Eberhart R. Particle swarm optimization. In: *Proceedings of the International Conference on Neural Networks*. NJ: Piscataway; 1995